# Genesis of Pre–Hurricane Felix (2007). Part II: Warm Core Formation, Precipitation Evolution, and Predictability

ZHUO WANG

*University of Illinois at Urbana–Champaign, Urbana, Illinois*

M. T. MONTGOMERY

*Naval Postgraduate School, Monterey, California, and NOAA/Hurricane Research Division, Miami, Florida*

T. J. DUNKERTON

*Naval Postgraduate School, Monterey, California, and NorthWest Research Associates, Bellevue, Washington*

### ABSTRACT

This is the second of a two-part study examining the simulated formation of Atlantic Hurricane Felix (2007) in a cloud-representing framework. Here several open issues are addressed concerning the formation of the storm's warm core, the evolution and respective contribution of stratiform versus convective precipitation within the parent wave's pouch, and the sensitivity of the development pathway reported in Part I to different model physics options and initial conditions. All but one of the experiments include ice microphysics as represented by one of several parameterizations, and the partition of convective versus stratiform precipitation is accomplished using a standard numerical technique based on the high-resolution control experiment.

The transition to a warm-core tropical cyclone from an initially cold-core, lower tropospheric wave disturbance is analyzed first. As part of this transformation process, it is shown that deep moist convection is sustained near the pouch center. Both convective and stratiform precipitation rates increase with time. While stratiform precipitation occupies a larger area even at the tropical storm stage, deep moist convection makes a comparable contribution to the total rain rate at the pregenesis stage, and a larger contribution than stratiform processes at the storm stage. The convergence profile averaged near the pouch center is found to become dominantly convective with increasing deep moist convective activity there. Low-level convergence forced by interior diabatic heating plays a key role in forming and intensifying the near-surface closed circulation, while the midlevel convergence associated with stratiform precipitation helps to increase the midlevel circulation and thereby contributes to the formation and upward extension of a tropospheric-deep cyclonic vortex.

Sensitivity tests with different model physics options and initial conditions demonstrate a similar pregenesis evolution. These tests suggest that the genesis *location* of a tropical storm is largely controlled by the parent wave's critical layer, whereas the genesis *time* and *intensity* of the protovortex depend on the details of the mesoscale organization, which is less predictable. Some implications of the findings are discussed.

## 1. Introduction

This is the second of a two-part study examining the numerically simulated formation of Atlantic Hurricane Felix (2007) in a cloud-representing framework. In Part I of this study (Wang et al. 2010, hereafter Part I) the simulation commenced during the wave stage of the precursor African easterly wave disturbance. Analysis of the real-case simulation pointed to a bottom-up development process within the parent wave's cyclonic "cat's eye" recirculation flow (or the wave pouch). The results broadly supported the hypotheses proposed by Dunkerton et al. (2009, hereafter DMW09) for tropical cyclone formation.

DMW09 proposed three new hypotheses linking synoptic, subsynoptic, mesoscale, and cloud-scale processes of the tropical troposphere. The cat's eye region within the easterly wave's critical layer was hypothesized to be

*Corresponding author address:* Zhuo Wang, Department of Atmospheric Sciences, University of Illinois, Urbana, IL 61801.
E-mail: zhuowang@illinois.edu

important in TC formation. In the first hypothesis (H1) wave breaking or roll up of the cyclonic vorticity and moisture near the critical surface in the lower troposphere provides a favorable environment for vorticity aggregation for TC formation; in the second (H2) the cat's eye is a region of quasi-closed Lagrangian circulation, where air is repeatedly moistened by convection and protected to some degree from dry air intrusion, which favors a predominantly convective type of heating profile; and in the third (H3) the parent wave is maintained and possibly enhanced by diabatically amplified mesoscale vortices within the cat's eye. The combination of H1–H3 was labeled the *marsupial paradigm* by DMW09 in order to distinguish the pregenesis flow topology, with its quasi-closed dome of recirculating fluid in the lower troposphere, from the well-known *stratified turbulence paradigm* in which layers of stratified quasi-two-dimensional turbulent flows slide across one another in seemingly random fashion. The cat's eye within the wave critical layer is thus dubbed the "wave's pouch" or simply "pouch." As noted by DMW09, westerly flow regimes in the upper tropical troposphere overlying easterly flows in the lower troposphere (in which easterly waves reside) are often uncorrelated with lower tropospheric development initially; therefore, the deep-layer vertical shear in any particular situation is equally likely to oppose genesis as to favor it. To summarize, (i) the tropical environment is generally hostile to tropical cyclogenesis, (ii) recirculating fluid in the lower troposphere promotes genesis when diabatically activated by a convecting protovortex within, and (iii) deep-layer vertical shear lends a stochastic ingredient to the problem, initially promoting development (if weak) or discouraging it (if excessive). As noted by DMW09 and others (e.g., Davis and Bosart 2003) deep-layer shear is eroded by an intensifying storm, so the stochastic ingredient is eliminated locally when development succeeds.

In Part I, the wave pouch was shown to provide a focal point for diabatic merger of convective vortices and their vortical remnants and to protect the moist air inside from dry air intrusion, providing a favorable environment for sustained deep convection. These findings directly support the above hypotheses, H1 and H2, respectively. Consistent with the findings of DMW09, the simulated storm formed near the center of the wave pouch via system-scale convergence in the lower troposphere and vorticity aggregation.[1]

In this paper we continue our theoretical/modeling study of Felix's cyclogenesis. We begin by answering the second and third questions posed in the introduction of Part I:

- How does a tropical depression-strength vortex form within a cold-core, lower tropospheric wave disturbance, and subsequently transition to a warm-core tropical cyclone?
- What are the relative roles of stratiform and convective processes in tropical cyclone formation and how does stratiform and convective precipitation evolve with time within the wave pouch?

The results reported here and in Part I reinforce a key idea of DMW09, that the *lower troposphere* plays an essential role in tropical cyclogenesis. At the synoptic scale, the precursor easterly wave has maximum amplitude near the jet level (600–700 hPa over the east Atlantic and about 850 hPa or lower over the west Atlantic). At the meso-$\alpha$ scale, the structure and temporal development of the critical layer varies from case to case, but we infer from the numerous events studied by DMW09 that the critical layer is aligned vertically (if not initially in some cases, certainly by genesis time) and that a connection is thereby established between the altitude of maximum disturbance (jet level) and the atmospheric boundary layer (the ultimate source of moisture to the interior). This connection serves to contain moisture lofted by deep convection or entrained from nearby sources (e.g., the ITCZ) within the pouch and to protect the pouch contents from dry air outside [e.g., the Saharan air layer (SAL)], which in turn favors deep convection and further development of the cyclonic circulation. As articulated in DMW09, positive feedbacks exist when low-level vorticity and deep moist convection are present simultaneously in the pouch; it is the cooperation of these feedbacks that provides an efficient pathway to storm development, especially in oceanic basins that are otherwise marginal or hostile to development. We say that the precursor or "parent" wave is *diabatically activated* when deep moist convection persists within the pouch, a likely sign of its underlying vortical organization and increasing (albeit local) dominance of convective cloud type. As shown in Part I, this development occurs near the center of the pouch, bringing together the original rotating convective elements at meso-$\gamma$ and their vortical remnants (straddling the artificial boundary between meso-$\gamma$ and meso-$\beta$) into coherent structure at meso-$\beta$, a scale (by definition) occupying only a fraction of the original pouch area at meso-$\alpha$. Part II of this study now reveals in more detail several aspects of this multifeedback loop pertaining to the simulated development of Felix (2007). To test the robustness of the findings reported in Part I, the sensitivity of the development pathway outlined in Part I to different model physics

---

[1] For a complete definition of all technical terms used herein, please consult DMW09 and the glossary therein.

TABLE 1. Resolution and physics options for the sensitivity tests. The last column lists the wave propagation speed as estimated from Hovmöller diagrams.

| Expt | Resolution | Model physics | Forcing data/ initialization time | Wave propagation speed |
|------|------------|---------------|-----------------------------------|------------------------|
| HR | 4 grids: 81–27–9–3 km | Kain–Fritsch cumulus, WSM6 microphysics, YSU PBL | ECMWF analysis, 0000 UTC Aug 29 | −9.8 |
| CR | 3 grids: 81–27–9 km | As in HR | As in HR | −10.4 |
| PBL2 | 3 grids: 81–27–9 km | As in HR but the Mellor–Yamada–Janjic PBL scheme is used | As in HR | −11.0 |
| MP1 | 3 grids: 81–27–9 km | As in HR but the Kessler scheme is used for microphysics | As in HR | −9.8 |
| MP2 | 3 grids: 81–27–9 km | As in HR but the Lin scheme is used for microphysics | As in HR | −10.1 |
| CU2 | 3 grids: 81–27–9 km | As in HR but the Betts–Miller–Janjic cumulus scheme is used | As in HR | −9.7 |
| 06Z | 3 grids: 81–27–9 km | As in HR and CR | ECMWF analysis, 0600 UTC Aug 29 | −9.4 |
| 12Z | 3 grids: 81–27–9 km | As in HR and CR | ECMWF analysis, 1200 UTC Aug 29 | −10.5 |
| GFS | 3 grids: 81–27–9 km | As in HR and CR | GFS analysis, 0000 UTC Aug 29 | −11.0 |

options and initial conditions is also examined. These sensitivity tests offer some new insights into the predictability of tropical cyclogenesis.

An outline of the remaining paper is as follows. The sensitivity tests are described in section 2. Section 3 examines the formation of the warm-core structure. The evolution of stratiform and deep convective precipitation and their respective contribution is examined in section 4. Section 5 presents a modest suite of sensitivity tests, followed by discussions and conclusions in section 6.

## 2. Model and sensitivity experiments

The Weather Research and Forecasting (WRF) model version 3.0 (Skamarock et al. 2005) was used in this study, and the model was described briefly in Part I. The control run has a four-grid nested domain configuration with horizontal grid spacing 81, 27, 9, and 3 km, respectively, initialized at 0000 UTC 29 August 2007, about 3 days prior to genesis. The initial conditions and lateral boundary forcing in the control run were derived from the ECMWF 6-hourly analyses with T106 resolution. The Kain–Fritsch scheme was used to represent cumulus convection in the two outer grids; in the two inner grids (9-km and 3-km resolution), cumulus convection was calculated explicitly at the grid scale. Other physics parameterizations used include the WRF single-moment, six-class microphysics (Hong and Lim 2006), Yonsei University (YSU) PBL scheme, Noah land surface scheme, Rapid Radiative Transfer Model (RRTM) longwave radiation scheme, and Dudhia shortwave radiation scheme.

To test the robustness of the results reported in Part I, sensitivity tests with different model physics and initial conditions were conducted. To save computational time, all sensitivity tests are carried out with three grids (81,

27, and 9 km; experiment HR is the high-resolution control run). Details of the sensitivity tests are provided in Table 1.

## 3. Formation of the warm-core structure

To examine the evolution of the thermodynamic structure, the radial–height distribution of the temperature deviation from the environment is constructed (Fig. 1). The temperature deviation is azimuthally averaged with respect to the pouch center (i.e., the center of the closed circulation in the comoving frame). At 23 h, relative to its surroundings the central region of the pouch has negative temperature difference below 600 hPa and positive temperature difference between 300 and 600 hPa. The thermal wind balance suggests that the cyclonic circulation is strongest at 600 hPa where the radial temperature difference changes sign. By 40 h the cold air mass below 600 hPa has been nearly eliminated near the pouch center, and the vortex begins to attain a warm-core structure. This transition to a warm core culminates sometime in the following 24 h, after genesis of a "tropical depression" but during the period of intensification to, and beyond, the threshold for a "tropical storm." At 64 h, the tropical storm (now approaching hurricane strength) has a well-defined warm-core structure with one temperature difference maximum of 4.5 K at 400 hPa and another of 3 K at 900 hPa.

It cannot be determined from the Felix simulation alone whether the transition to a fully warm core must await the official designation as tropical storm in all such cases, but the idea is plausible, based on the hurricane model of Emanuel (1986) in which isosurfaces of (i) absolute angular momentum, (ii) saturation equivalent potential temperature, and (iii) mass streamfunction of
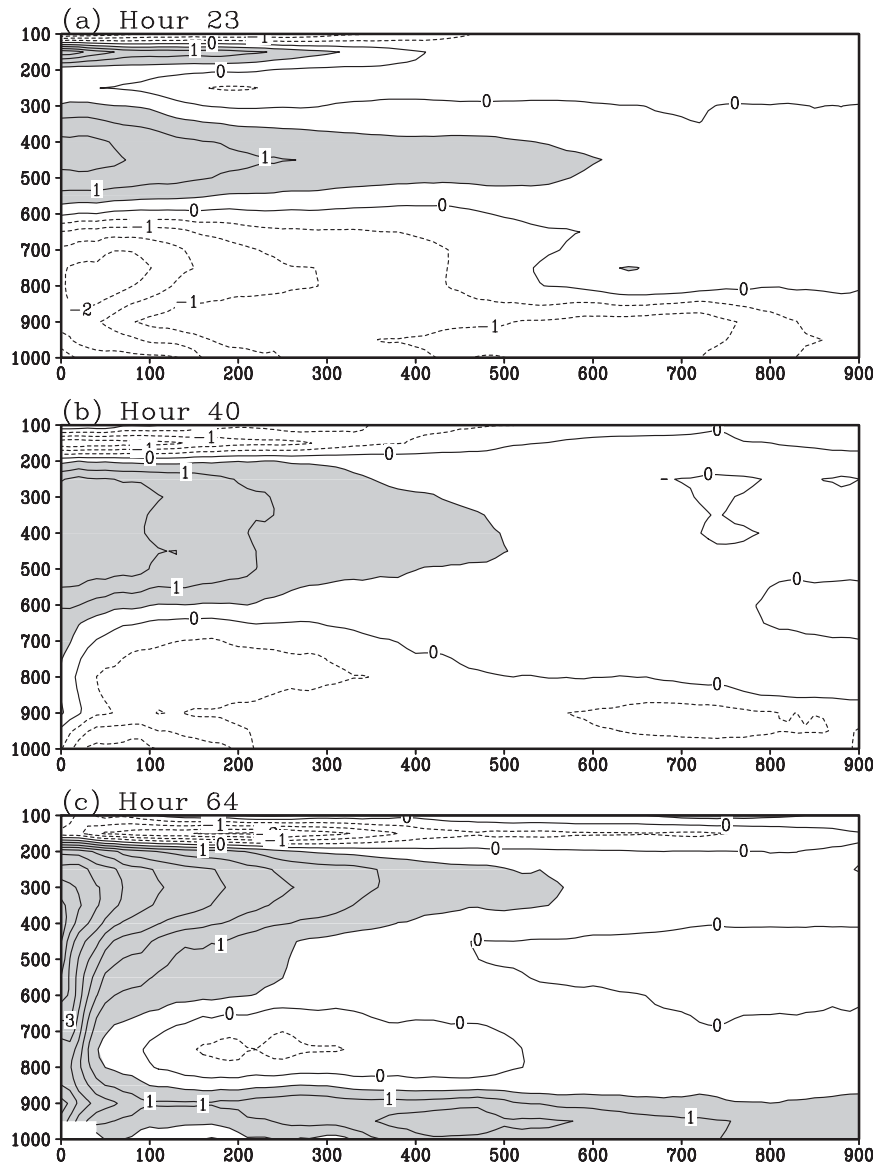
FIG. 1. Vertical cross section of temperature difference from the environment (1200 km away from the pouch center). The temperature difference is azimuthally averaged with respect to the pouch center. The abscissa is radius (km) and the ordinate is pressure (hPa). Contour intervals are 0.5 K, and positive differences larger than 0.5 K are highlighted by shading.

overturning transverse or "secondary" circulation are congruent in the radial–height plane. These surfaces radiate outward with increasing height above the boundary layer, a configuration seen in the asymptotic, but not initial, stage of storm development (e.g., Schubert and Alworth 1987; Wirth and Dunkerton 2006). By hydrostatic and gradient balance, outward radiation of *m* surfaces signifies a decreasing intensity with increasing altitude and warm-core structure above the boundary layer. It is helpful to note that the temperature tendency in the moist inner core is not the result of deep convective

heating alone, but a relatively small residual between convective heating and the cooling of adiabatic ascent. This residual tends to zero asymptotically with time (aside from small vacillations in the steady state). The temperature tendency is more simply regarded as the preservation of hydrostatic and gradient balance in response to the evolving (and highly complex) vorticity dynamics. Development of the classic structure from weakly perturbed initial conditions evidently involves an interplay between boundary layer processes, communication of boundary layer thermodynamic properties to
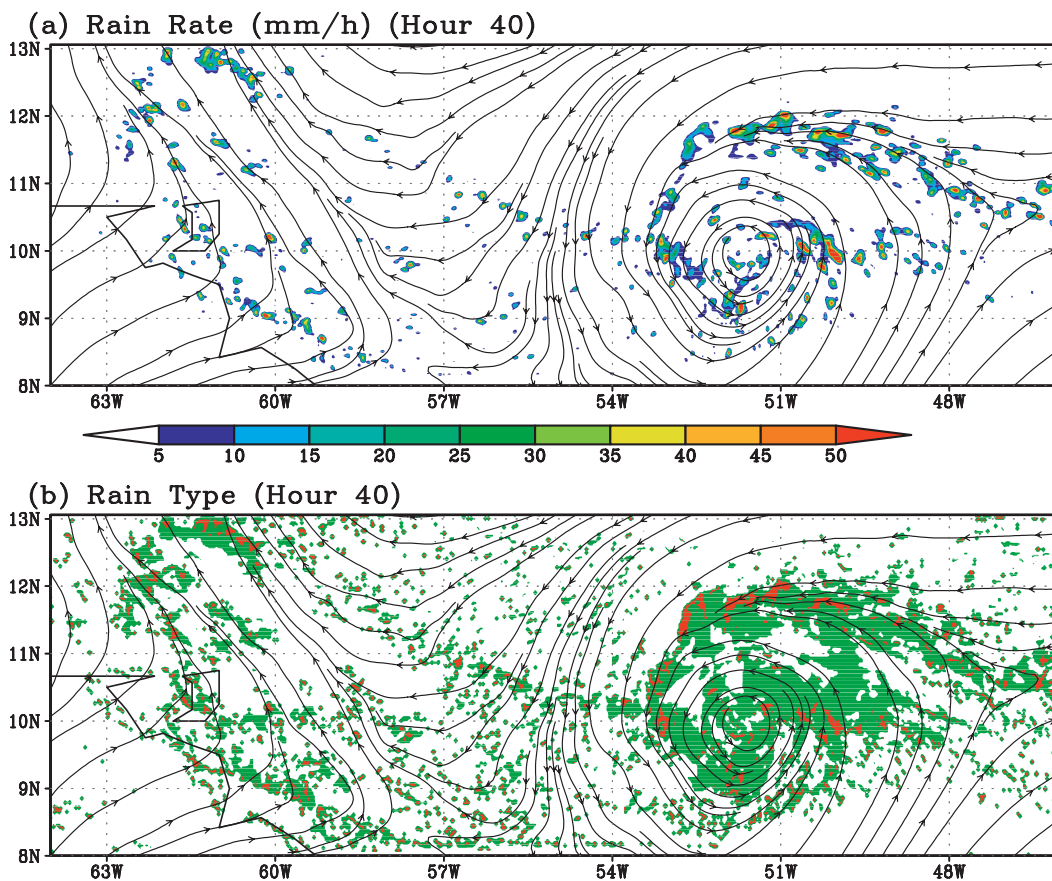
FIG. 2. (a) Rain rate and (b) rain type at 40 h. The color in (b) represents stratiform (green) and convective (orange) precipitation.

the upper troposphere, and nonlinear advection by the secondary circulation of the primary circulation's absolute angular momentum in the interior (i.e., above the boundary layer). Azimuthal asymmetries add complications of their own. Our simulation of Felix illustrates nicely the generic transition from the cat's eye structure of a wave's pouch to a more intense and localized storm with increasing circular symmetry.

## 4. Stratiform versus deep convective precipitation

### a. Precipitation partition

Precipitation is partitioned as convective and stratiform following Tao et al. (1993) and Braun et al. (2010). First, grid points with rain rates twice as large as the average of their nearest four neighbors are identified as convective cell cores. If a grid point is designated as a convective cell core in this way, then its nearest neighbors (within one grid distance) are also designated as convective. Second, all grid points with surface rainfall rates greater than 25 mm h$^{-1}$ are categorized as convective. To identify convective columns in which significant

precipitation is not reaching the surface, columns with maximum upward vertical motions greater than 5 m s$^{-1}$ or cloud liquid water below the melting level larger than 0.5 g kg$^{-1}$ are also designated as convective. All remaining grid columns with surface precipitation greater than 0.1 mm h$^{-1}$ are categorized as stratiform, and all the other grid columns are considered as nonprecipitating. Our tests show that this method is sensitive to the grid size and thresholds used to distinguish the convective and stratiform rainfall. For example, if a 16-grid-point average, instead of one of 4 grid points, is used to identify convective cell cores, many more grid points will be categorized as convective. To avoid overestimating the convective contribution, some of thresholds used in this study are higher than in Tao et al. (1993) or Braun et al. (2010). Such calibrations are needed because the method is not well posed mathematically and is attempting to classify precipitation behavior without explicit metrics [such as updraft velocity, convective available potential energy (CAPE), and downdraft CAPE (DCAPE)] better suited for this purpose. Such metrics obviously contain subgrid variability that cannot be evaluated from the

numerical output because the model resolves the cloud system, not individual drafts. Our objective is to examine the quantitative evolution of stratiform and convective precipitation and their relative importance. With the preceding caveats, we believe the algorithm used is adequate for the purpose of understanding storm development and organization in the pregenesis stage, which (as will be shown here) are insensitive to variations of grid spacing less than 9 km.

Figures 2a and 2b show a snapshot of the distribution of the precipitation rate and precipitation types superimposed on the translated streamlines at 40 h. Both precipitation rate and precipitation types are derived from the output of the innermost grid in the high-resolution control experiment in which convection is resolved on grid scale explicitly. The distribution of the convective precipitation (Fig. 2b) has a pattern similar to the distribution of a high precipitation rate (Fig. 2a), which suggests that it is the major contributor to a high precipitation rate. Figure 2b shows also that stratiform precipitation covers a much larger area than convective precipitation. Although convection is not limited to the pouch, organized convection is mainly confined within the pouch and along the outward-moving convective lines.

To examine the evolution of stratiform versus convective precipitation, the radial distributions of the two types of precipitation with respect to the pouch center are derived. The top panels of Fig. 3 show the azimuthal fraction covered by convective and stratiform precipitation, and the bottom two panels show the contribution of convective and stratiform processes to total rain rate. Similar to Fig. 1, all quantities are averaged azimuthally with respect to the pouch center. For example, the value 80% in Fig. 3a at 60 h along the radius 100 km means 80% of the area in the 10-km annulus (with inner and outer radii of 95 and 105 km, respectively) is covered by stratiform precipitation.

The top panels in Fig. 3 show that stratiform precipitation covers a much larger area than convective precipitation. Even when the storm reaches hurricane intensity in the later stage of the simulation, stratiform precipitation still covers more than 50% of the area. Although convective precipitation covers only a small fraction of area within the pouch, its coverage increases with time near the pouch center. Furthermore, since most heavy precipitation areas are convective, the convective process makes a comparable contribution to total rain rate as stratiform at the early stage (before 40 h) and a larger contribution at the later stage within the 100-km radius (bottom panels).

Figure 3 suggests also that the deep convection is sustained around the pouch center. Close inspection of the figure indicates that convection is not always present

at the origin even though that is exactly where vorticity aggregates and amplifies most, as noted earlier. Away from the pouch center, convective precipitation is more transient and has an outward propagation along one or more spiraling convective lines. These lines are associated with gust fronts, gravity waves, or vorticity boundaries (DMW09) that can initiate new convective cells by lifting parcels of high entropy. The large-scale flow plays a role in organizing these lines or modifying their propagation (e.g., when they appear quasi-parallel to streamlines, as seen north of center) via filamentary straining of ambient vorticity, or "wave capture" (Bühler and McIntyre 2005), of outward propagating gravity waves and gust fronts.

### b. Transverse (secondary) circulation

To examine the respective contribution of the stratiform and convective processes to the spinup of the storm, vertical velocity and divergence associated with the stratiform and convective precipitation are calculated within the $2° \times 2°$ box following the pouch center. To show the relative contribution of each process, the total stratiform and convective vertical velocity/divergence are averaged over the entire $2° \times 2°$ box instead of being area weighted. In other words, taking the average over the entire box, wherein some or many cells may be nonprecipitating, effectively dilutes the more vigorous velocity and divergence characteristic of the convective or stratiform columns themselves.

The convective vertical velocity is shown in Fig. 4a. Rising motion extends from the surface throughout the troposphere, with a maximum around 700 hPa early in the simulation elevated to 600 hPa later. A secondary maximum is located at 300 hPa. A close look at the vertical structure of vortical hot towers (VHTs) shows that some VHTs, especially the most vigorous ones, have a peak vertical velocity around 300 hPa. Therefore, the secondary maximum at 300 hPa does not necessarily suggest an overestimate of the convective contribution by including some stratiform precipitation.[2] The convective divergence is shown in Fig. 4c, with convergence below 700 hPa and divergence above, which is typical of a convective divergence profile (CDP) (e.g., Mapes and Houze 1995). The maximum convergence occurs in the

---

[2] The opposite is more likely, namely that the convective contribution is underestimated in these figures. As already noted, a longer horizontal scale (or a larger area average) separating the two categories greatly increases the number of convective columns. The contrast between the two categories may be enhanced, not diminished, by including more cells in the convective category, provided that the convective category is not broadened too much in horizontal scale.

boundary layer, and there are two divergence maxima, one at 500 hPa and one at 150 hPa.

The stratiform vertical velocity and divergence are shown in Figs. 4b and 4d. Over the stratiform grid points, there is upward (downward) motion above (below) 600 hPa. This structure corresponds to the stratiform divergence profile (SDP): convergence in the middle levels (300–700 hPa) and divergence in the upper and lower levels. Note that the low-level convergence associated with deep convection is much stronger than the low-level divergence associated with the stratiform processes. The net convergence in the lower troposphere spins up the low-level circulation. In the middle levels (400 to 600 hPa), the stratiform convergence more than offsets the convective divergence. The net convergence profile (Fig. 13a of Part I) thus has a deep convergence layer from the surface up to 300 hPa with two maxima, one in the boundary layer and the other around 400 hPa. These findings are consistent with the idealized experiments of tropical cyclogenesis by Montgomery et al. (2006), who showed two main inflow branches. The low-level inflow/convergence that spins up the near-surface circulation is associated with deep convection. The mid- to upper-level inflow/convergence that contributes to spinning up a deep cyclonic circulation is associated with stratiform processes and likely also vigorous VHTs (see footnote 2). Both stratiform and convective processes contribute to the upper-level divergence. It is of interest to point out that, while the stratiform and convective rain rates generally increase with time, the convective rain rate increases more in a relative sense (see Figs. 3c and 3d). The net divergence profile consequently becomes dominantly convective (see Fig. 13a of Part I and Fig. 4 of this study), favoring cyclonic spinup of the low-level circulation.

Since diabatic heating plays an important role in maintaining the transverse circulation (e.g., Kurihara 1975; Montgomery et al. 2006), changes in the heating profile may lead to changes in the transverse circulation. Figure 5 shows the azimuthally averaged radial, vertical, and tangential velocity fields at the different stages.

At the wave stage (23 h, top panels in Fig. 5), the radial velocity has a quadrupole structure with inflow below 500 hPa and outflow above within an 800-km radius and the reversed pattern outside. The updraft prevails throughout the troposphere near the center of the pouch, while around 100-km radius the vertical velocity profile is a mix of convective and stratiform structure, with updrafts above 600 hPa and downdrafts below. Deep downdrafts are found around the 800-km radius, consistent with the upper-level convergence and low-level divergence there. Tangential wind shows a maximum of $\sim$10 m s$^{-1}$ at 600 hPa about 150 km away from the

pouch center, and anticyclonic circulation is present at the upper level ($\sim$250 hPa) with the radius of maximum anticyclonic wind about 700 km.

Around the genesis time (40 h, middle panels in Fig. 5), the strong tropospheric deep updrafts expand to the 200-km radius. The stratiform downdraft is offset by the convective updrafts within the central region of the pouch. The transverse circulation begins to attain the in–up–out structure. Strong inflow is confined below 800 hPa and starts as far as 900 km away from the pouch center. The outflow also becomes stronger and is confined around 200 hPa. Different from the typical transverse circulation of a tropical storm, weak inflow is also found in the midtroposphere (below 400 hPa) near the pouch center but is much weaker and less expansive than the low-level branch; it is also disrupted by outflow at some locations. In comparison with the early wave stage, the major change in the tangential wind is the low-level intensification. The maximum tangential wind appears to move downward to about 800 hPa with a small amplification of the maximum tangential wind. This is consistent with Fig. 1, which suggests that the vortex has begun to attain a warm-core structure at this stage. The translated streamlines in Part I of this study (see Fig. 9 in Part I) show that the wave pouch becomes more circular. This may cause the apparent shrinking of the vortex, as indicated by 4 or 6 m s$^{-1}$ isotachs.

At the storm stage (bottom panels in Fig. 5), the transverse circulation has established the typical in–up–out structure. Outward flow starts above 900 hPa near the storm center. A strong inflow is mainly confined in the lower troposphere, with a weaker secondary inflow maximum around 400 hPa at the 400-km radius. From 40 to 64 h, the maximum tangential wind increases from 10 to 26 m s$^{-1}$ and descends from 800 hPa to $\sim$900 hPa. The storm has established a typical warm-core structure. The radius of maximum tangential wind decreases significantly from 150 km to less than 50 km. The simulated storm is of small size, as that observed.

## c. Relation of cloud type, transverse circulation, and vortical organization

The preceding discussion, and that to follow in section 5 (as well as the diagnosis in Part I), pinpoints the central region of the wave's pouch as the most probable location of storm development. A relationship evidently exists between this "sweet spot" acting as the favored locus of cyclonic vorticity aggregation while at the same time promoting the eventual dominance and persistence of deep convective cloud type. These twin developments (of vortical and cloud organization) are, we believe, closely related, and exhibit two conceptually distinct
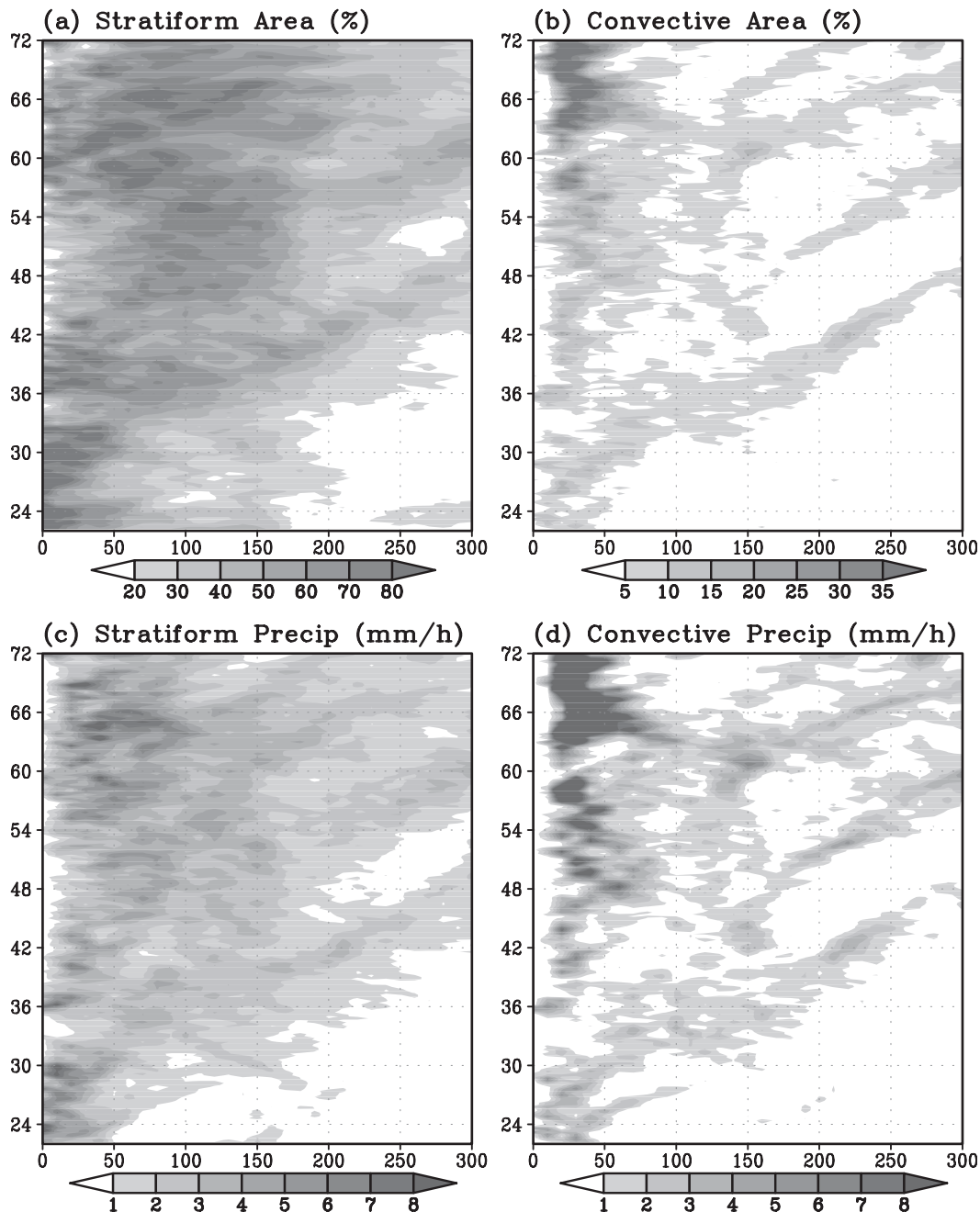
FIG. 3. Time–radial evolution of the (left) stratiform and (right) convective precipitation, showing (top) area coverage (%) by each rain type and (bottom) the azimuthal mean rain rate (mm h$^{-1}$) associated with each rain type. The abscissa is radius (km) with respect to the wave pouch center, and the ordinate is time (h).

aspects (Montgomery et al. 2006). First, convective plumes, which happen to develop in a location already rich in cyclonic vorticity, are likely to further amplify the cyclonic vorticity through vortex-tube stretching, leading to the formation of VHTs and their possible diabatic merger into larger coherent structures and even larger, more persistent, remnant vortices in the lower

to midtroposphere. Once convection ceases, the latter may continue to merge adiabatically. Second, an ensemble of active, corotating VHTs near the pouch center projects onto the azimuthally averaged interior diabatic heating, which drives the familiar in–up–out Eliassen secondary circulation. In the pregenesis stage and for several hours thereafter, the axisymmetric circulation has
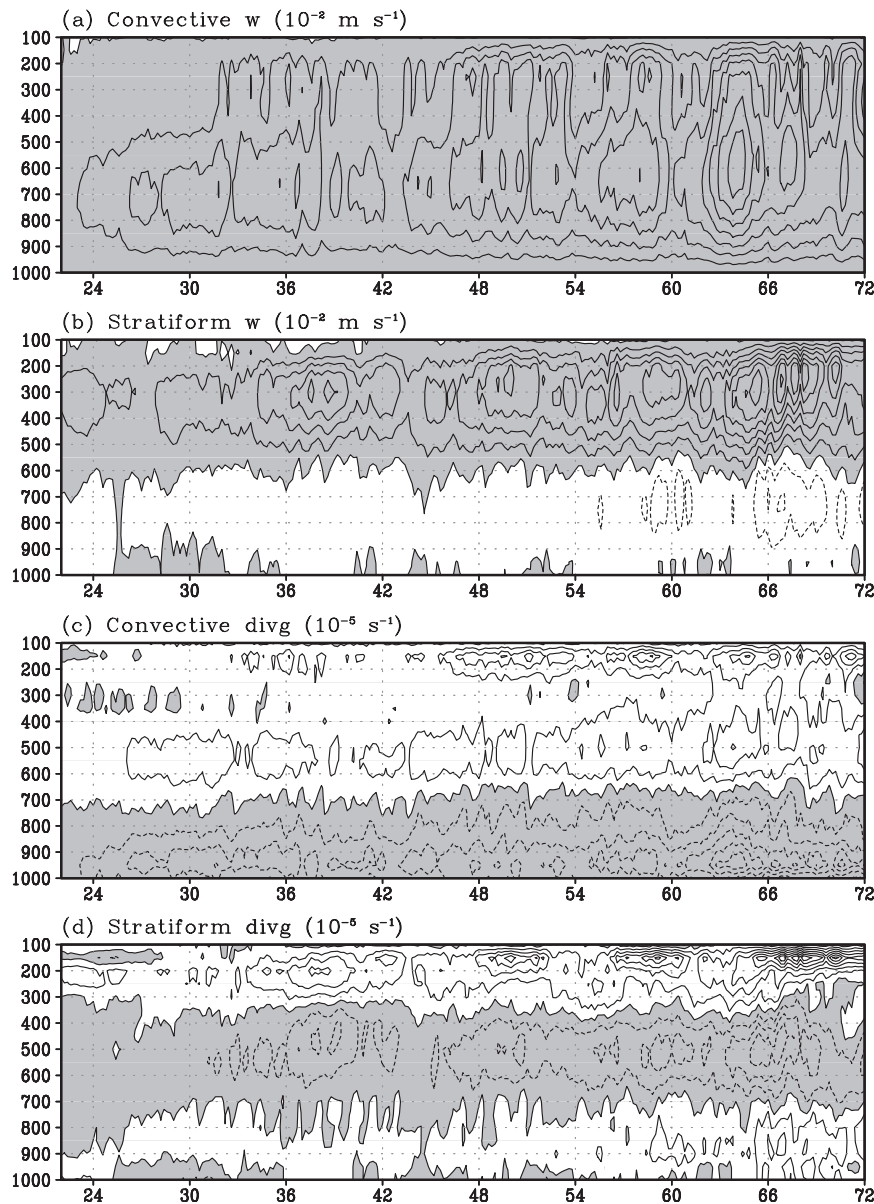
2°X2° Box Average



FIG. 4. Time–vertical section of the (a),(b) area-average vertical velocity [contour interval (CI) $4 \times 10^{-2}$ m s$^{-1}$] and (c),(d) divergence (CI $= 2 \times 10^{-5}$ s$^{-1}$) in the convective and stratiform regions in the 2° × 2° box following the wave pouch. Upward motion and convergence are highlighted in gray. The abscissa is time (h), and the ordinate is pressure (hPa).

not yet achieved its classic structure (as articulated above; Emanuel 1986) but is evolving temporally toward that state in response to the imposed diabatic heating (Wirth and Dunkerton 2006). These distinct aspects are compatible but not entirely interdependent. For example, the Eliassen circulation requires a persistent axisymmetric component of heating (VHTs active at one or more azimuths simultaneously) whereas adiabatic merger of vortical remnants may continue whether or not such heating is temporally continuous. Adiabatic merger remains a viable mechanism in this context provided that the Okubo–Weiss (OW) parameter is positive locally.

As noted in Part I, it stands to reason that the radially inward component of the Eliassen circulation aids cyclonic vorticity aggregation in the lower troposphere as well as spinning up the low-level circulation. In this sense,
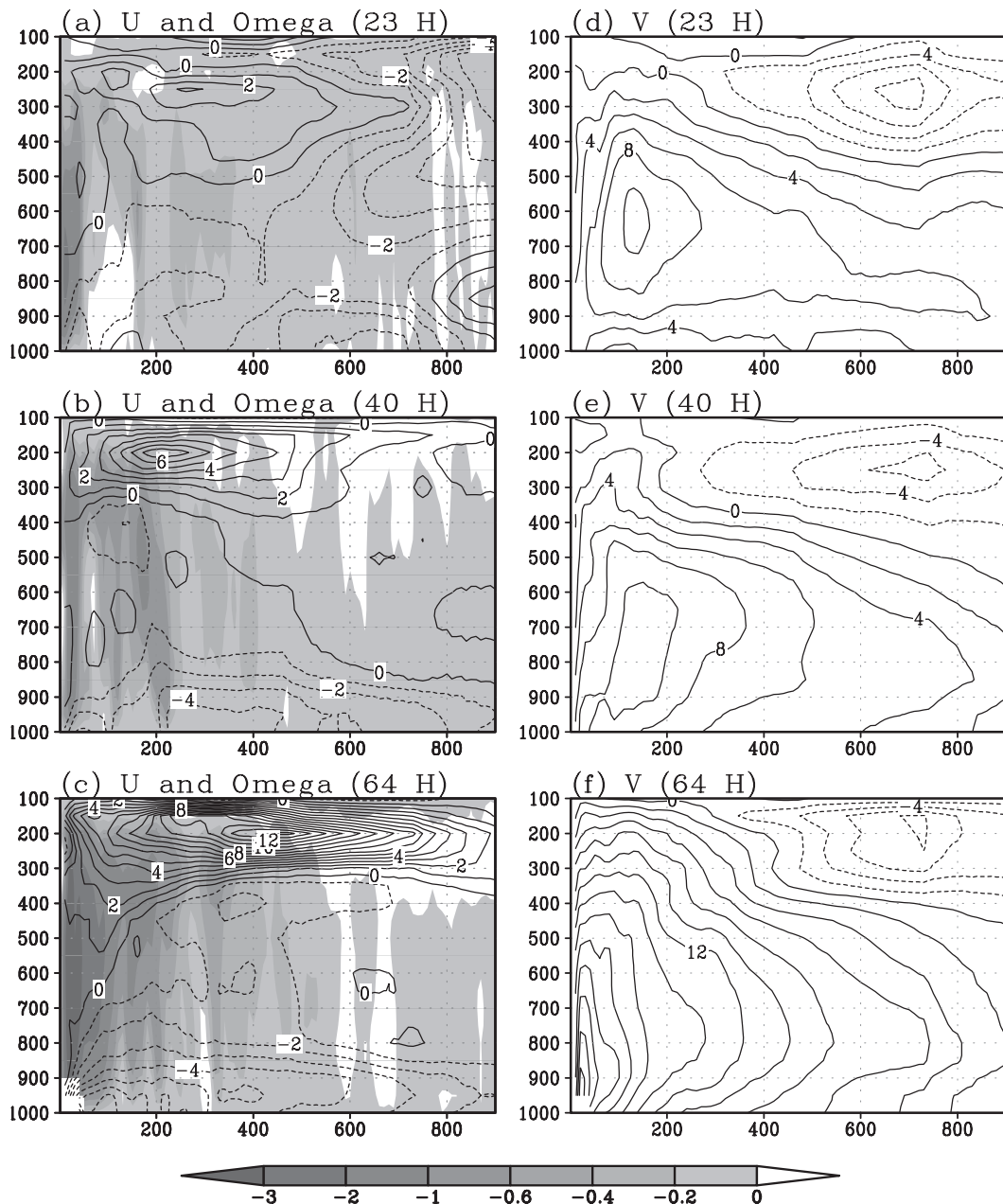
FIG. 5. Vertical cross section of the (left) radial velocity (contours; CI = 1 m s$^{-1}$) and vertical velocity in isobaric coordinates (shading, Pa s$^{-1}$) and (right) tangential velocity (CI = 2 m s$^{-1}$) at (top) 23 h, (middle) 40 h, and (bottom) 64 h. The abscissa is radius (km), and the ordinate is pressure (hPa).

the distinct aspects of vortical organization are not merely compatible; they are synergistic. But, what about the synergy between vorticity and cloud type, if any? And, what is special about the pouch center in this respect? Given that deep moist convection dominates and persists near the sweet spot, *why* does it dominate and persist?

To understand the spatiotemporal organization of clouds and cloud type it is important to note that stratiform cloud in precipitating regions is generally ubiquitous

in all but the most saturated environments. Stratiform cloud does not decrease in time; rather, the convective rain rate becomes dominant near the pouch center. This does not mean that convection is absent elsewhere; our control simulation, in fact, shows transient, vigorous deep convection aligned along the boundaries of the pouch in what are ostensibly filamentary or "frontal" zones with negative OW parameter on the large scale. It is clearly seen that storm development near the pouch center
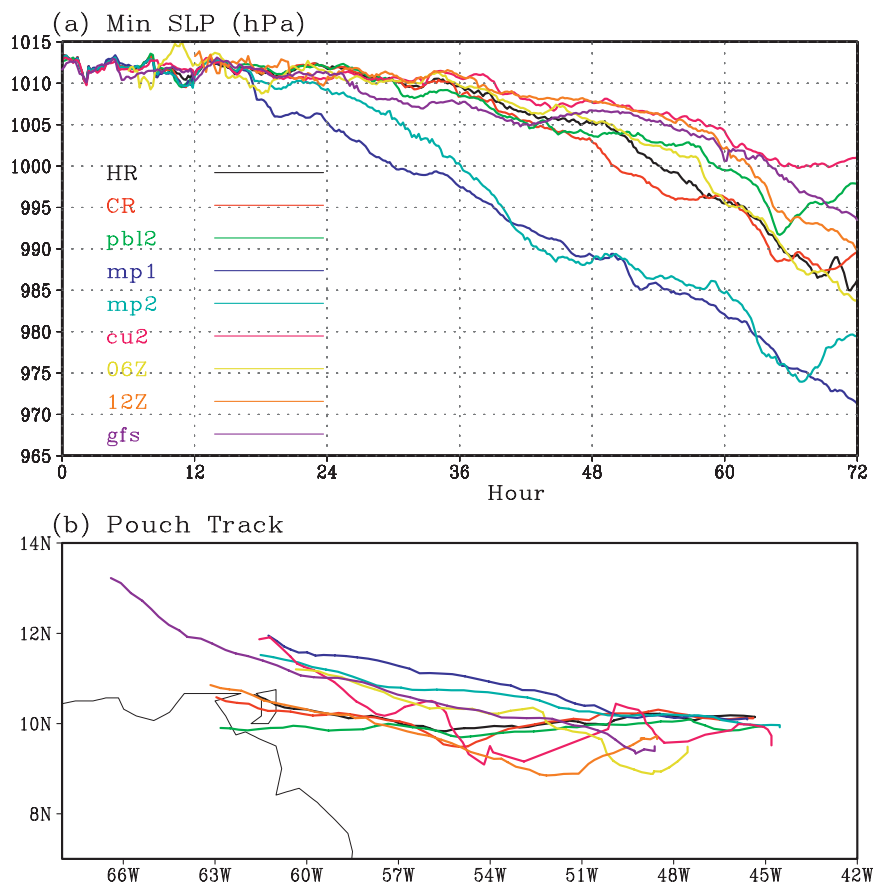
FIG. 6. (a) Time series of the minimum sea level pressure (SLP) from the nine simulations (derived from the 9-km resolution grid outputs). (b) The track of the wave pouch in the nine simulations from 22 to 72 h. Different colors are used to represent different experiments.

requires not only deep convection but also a persistent *rotational organization* of deep convection here. Not surprisingly, this sweet spot represents the optimum location for the first two hypotheses of DMW09 and their constructive interplay prior to genesis.

It should be noted that everything said thus far regarding the interaction of vorticity and deep moist convection applies to a loosely organized collection of elements in the genesis stage prior to storm intensification. We have said that "waves precede vortices" (DMW09) in the sense that the parent wave and its pouch, diabatically activated by deep convection within, interact synergistically with one or more embryonic protovortices, the strength of which (prior to intensification) remain one or two orders of magnitude weaker than a hurricane. The cat's eye pattern of streamlines cannot be attributed to a hurricane, or row of hurricanes, that does not yet exist. This point will become clearer in the following section, wherein alternatives to the control experiment are examined.

Evolution toward a *locally circular geometry* from the initial cat's eye structure of the parent wave critical layer

is arguably the most important factor governing the mutual organization of cyclonic vorticity and deep convection, and the prevalence of convective cloud type in the region of strongest vorticity. Recirculation near the pouch center and its beneficial effects on moist thermodynamics become increasingly certain as tangential winds accelerate; the recirculation time decreases and the inward advection of axial angular momentum increasingly controls the tangential acceleration as the circular geometry takes hold. To appreciate why this interplay succeeds, even in marginal basins, it is helpful to imagine how the feedback loop may be frustrated: for example, by horizontal strain/shear deformation (negative OW parameter), vertical shear strong enough to tilt buoyant plumes off-center, or a burst of large-scale downdraft caused by evaporative cooling in the interior.

## 5. Predictability of tropical cyclogenesis

Figure 6a shows the time series of the minimum sea level pressure (SLP) for the nine simulations, all derived

from the 9-km resolution grid outputs. The simulations have quite different intensity evolution, with the minimum SLP at 2300 UTC 31 August (72 h in experiment HR) ranges from 1002 to 972 hPa. The simulation with the Betts–Miller–Janjic cumulus scheme (CU2) produces the weakest storm, and the simulations with Kessler warm rain microphysics (MP1) and Lin microphysics (MP2) (Lin et al. 1983) produce the strongest storms. Previous studies have reported that the Lin scheme tends to overpredict precipitation and storm intensity (Fovell and Su 2007; Otkin et al. 2006), and Montgomery et al. (2009) found that the Kessler warm rain scheme favors an early storm development. The intensity evolution in experiments HR, CR (as in HR but with coarse resolution), and 06Z (as in CR but initialized at 0600 UTC 29 August) are quite similar, and the storm in experiment 12Z, which is initialized at 1200 UTC 29 August, is slightly weaker. The simulated storm in experiment PBL2 (with the Mellor–Yamada–Janjic PBL scheme) undergoes a rapid intensification by 64 h and then weakens as the storm moves over land. Overall, stronger sensitivity of the storm intensity is due to microphysics and cumulus parameterizations rather than model resolution or initial condition.

The pouch tracks from 2100 UTC 29 August to 2300 UTC 31 August (22–72 h in the control simulation) are shown in Fig. 6b. The propagation speed of the wave pouch is estimated based on Hovmöller diagrams of meridional velocity and ranges from $-9.4$ to $-11.0$ m s$^{-1}$, as listed in Table 1, faster than that observed. The pouch track is determined by manually selecting the pouch center in the comoving frame of reference. By 2100 UTC 29 August, a pouch formed at 850 hPa in all the simulations except the 12Z run, in which an 850-hPa pouch formed at 2200 UTC 29 August. In CU2 (with the Betts–Miller–Janjic cumulus scheme), the simulation is hyperactive with multiple strong vortices within the pouch (see the upcoming discussion of Fig. 7). The pouch structure and track undergo large variations as the strong vortices interact with each other but fail to coalesce. By the end of the simulation (2300 UTC 31 August), the pouches in the ECMWF-driven simulations are within a 2° latitude range. As an outlier, the wave pouch in experiment GFS [as in CR but forced by Global Forecast System (GFS) analysis data] propagates much faster and curves farther northward. This suggests that the pouch track is more sensitive to the large-scale forcing than to the model physics or initial condition. It is noteworthy that the location of storm development in GFS follows the center of the wave pouch even when the latter's location is grossly incorrect.

To illustrate vorticity aggregation within the wave pouch, Fig. 7 shows the 850-hPa maximum relative vorticity (shading) along each latitude between 7° and 14°N

from 12 to 72 h, superimposed on the pouch track (black curves). As shown in the diagrams, the pouch is a cyclonic vorticity-rich environment, and mesoscale cyclonic vortices (or VHTs in experiment HR) usually form within 2° to 3° from the pouch center. Vorticity aggregation is best illustrated in experiment HR. At the early stage of the calculation, multiple vortices and their vortical remnants, as represented by local vorticity maxima, are present and compete within the pouch. They rotate around and move toward the center of the pouch, eventually forming an intense vortex near the pouch center with a larger spatial scale than the individual remnant convective vortices. The vorticity aggregation in experiments CR and PBL2 is similar to that in HR except that mesoscale vortices are of a larger spatial size and the storm, by the end of the simulation, is weaker than that in HR. In the warm rain simulation (MP1), the dominant vortex forms much earlier and the final storm has a stronger intensity and larger spatial scale. In experiment MP2 (with the Lin microphysics scheme), there are fewer mesoscale vortices and a dominant strong vortex forms by 36 h, whereas in CU2, more vortices are present and they fail to consolidate by the end of the simulation period. In experiments PBL2 and HR, the wave pouch track is nearly zonal along 10°N, whereas in the other runs the wave pouch track turns slightly northward.

The modest sensitivity of the pouch track to model physics and initial conditions is similar to previous studies highlighting storm track sensitivities to model physics (e.g., Fovell and Su 2007), and some of the differences may be due to intrinsic chaotic effects associated with the deep convective processes as well (Nguyen et al. 2008). All of the developing cases, however, demonstrate a similar pregenesis evolution: The pouch center is the focal point of vorticity aggregation, and a tropical depression vortex tends to form at this sweet spot via diabatic merger of convective vortices and their vortical remnants. The multiple-vortex activity exhibited prior to the attractor-type behavior is reminiscent of T. Fujita's infamous "suction vortices" first hypothesized from retrospective tornado damage surveys (Fujita 1992). As a tribute to his pioneering research in mesometeorology, this type of diagram will be referred to as a "Fujita diagram."

Note that VHTs have the lifetime $O(1 \text{ h})$ (vortical remnants can last a much longer time). The numerical model simulation of VHTs is highly sensitive to model initial conditions and model physics. The deterministic feature of the genesis location is in sharp contrast with the unpredictable nature of VHTs and suggests that the upscale vorticity aggregation is quantitatively guided by the synoptic or meso-$\alpha$ scale circulation. This explains why the genesis location can be predicted with reasonable
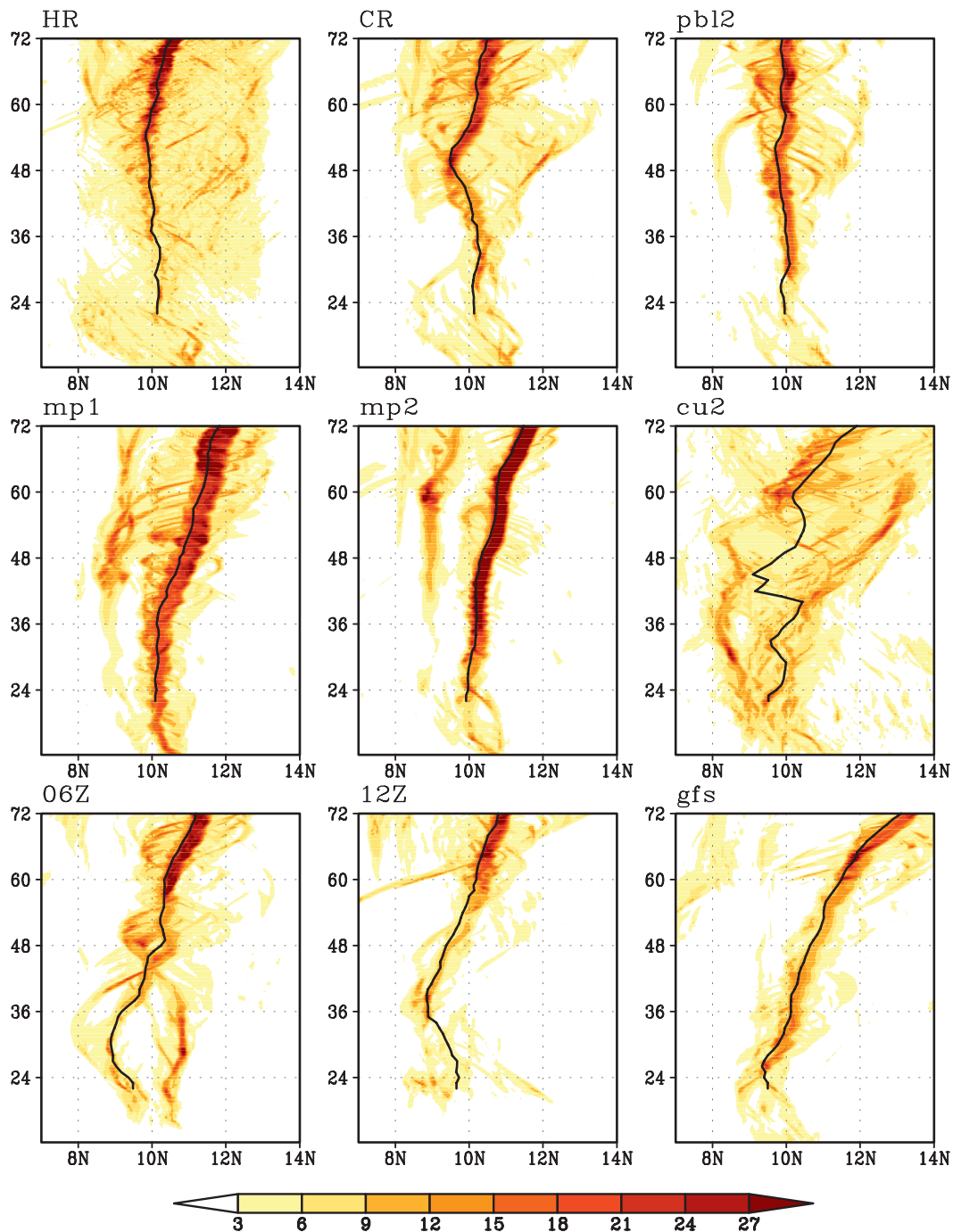
FIG. 7. Time evolution of the 850-hPa maximum relative vorticity vs latitude derived from the 9-km resolution grid. The *x* axis indicates the latitude of the vorticity maximum and the *y* axis is time from 12 to 72 h. Shading indicates intensity of the vorticity ($10^{-4}$ s$^{-1}$), and the thick black curve is the track of the wave pouch as determined from the translated streamlines of the 27-km resolution grid.

skill even using coarse-resolution global model products (Wang et al. 2009). By contrast, the genesis time is less predictable because the intensity of the system depends on mesoscale processes. This is analogous to the fact that

the hurricane *intensity* forecast is more challenging than the *track* forecast.

The theories of the ideal dry Rossby-wave critical layer (Killworth and McIntyre 1985, and references

therein) predict that the cat's eye precedes (logically and chronologically) the redistribution of PV within, and the advecting flow within the critical layer does not depend to leading order on the PV redistribution itself. On the other hand, for moist Rossby waves the simulated sensitivity of the wave pouch to initial conditions and model physics (Fig. 6), though modest compared to that of large-scale forcing as seen in the GFS run, suggests that mesoscale processes within the pouch have feedback to the synoptic or meso-$\alpha$ scale circulation. The genesis problem is intrinsically nonlinear owing to the multiscale interactions. Further work examining the multiscale interaction facets of the problem is warranted.

## 6. Conclusions

To obtain an improved understanding of the role of stratiform and convective processes in the genesis sequence of the pre-Felix disturbances examined in Part I of this study, precipitation in the high-resolution simulation was categorized as stratiform and convective, following Tao et al. (1993). It was found that sustained convection occurs near the pouch center. Although stratiform precipitation covers a larger fraction of area within the pouch even at the storm stage, deep convection makes a comparable (larger) contribution to the total rain rate at the pregenesis (storm) stage. Both stratiform and convective precipitation increase with time, but the convergence profile becomes dominantly convective because of the relatively large increase of convective precipitation near the pouch center.

Sensitivity tests with different model physics and initial conditions were performed to test the robustness of the results. All but one of the experiments contained a parameterization of ice microphysics. The simulated storm's intensity was more sensitive to the model physics than to the model resolution or initial conditions. By contrast, the pouch track was more sensitive to the lateral boundary forcing. Despite differences among the sensitivity tests, the basic picture remains the same: the tropical storm forms near the pouch center where vorticity aggregation is most efficient. This deterministic characteristic of the genesis location is in sharp contrast with the limited predictability of the storm intensity. It suggests that the diabatic merger of convective vortices and their vortical remnants is largely controlled by the parent wave's pouch (the guiding hand) while the intensification of the protovortex depends on mesoscale processes, which are intrinsically less predictable. This provides a dynamical explanation as to why tropical cyclogenesis location (not time) can be predicted using coarse-resolution global model products (Wang et al. 2009). On the other hand, the modest sensitivity of the wave pouch (formation, propagation speed, and track) to the model physics and initial conditions suggests that mesoscale convective processes have some feedback to the synoptic and meso-$\alpha$ scale motions, especially after a protovortex has formed. This is consistent with hypothesis H3 of DMW09.

REFERENCES

Braun, S. A., M. T. Montgomery, K. Mallen, and P. D. Reasor, 2010: Simulation and interpretation of the genesis of Tropical Storm Gert (2005) as part of the NASA Tropical Cloud Systems and Processes Experiment. *J. Atmos. Sci.,* **67,** 999–1025.

Bühler, O., and McIntyre, 2005: Wave capture and wave–vortex duality. *J. Fluid Mech.,* **534,** 67–95.

Davis, C. A., and L. F. Bosart, 2003: Baroclinically induced tropical cyclogenesis. *Mon. Wea. Rev.,* **131,** 2730–2747.

Dunkerton, T. J., M. T. Montgomery, and Z. Wang, 2009: Tropical cyclogenesis in a tropical wave critical layer: Easterly waves. *Atmos. Chem. Phys.,* **9,** 5587–5646.

Emanuel, K. A., 1986: An air–sea interaction theory for tropical cyclones. Part I: Steady-state maintenance. *J. Atmos. Sci.,* **43,** 585–605.

Fovell, R. G., and H. Su, 2007: Impact of cloud microphysics on hurricane track forecasts. *Geophys. Res. Lett.,* **34,** L24810, doi:10.1029/2007GL031723.

Fujita, T. T., 1992: *Mystery of Severe Storms.* Chicago University Press, 298 pp.

Hong, S.-Y., and J.-O. Lim, 2006: The WRF single-moment 6-class microphysics scheme (WSM6). *J. Korean Meteor. Soc.,* **42,** 129–151.

Killworth, P. D., and M. E. McIntyre, 1985: Do Rossby-wave critical layers absorb, reflect or overreflect? *J. Fluid Mech.,* **161,** 449–492.

Kurihara, Y., 1975: Budget analysis of a tropical cyclone simulated in an axisymmetric numerical model. *J. Atmos. Sci.,* **32,** 25–59.

Lin, Y.-L., R. D. Farley, and H. D. Orville, 1983: Bulk parameterization of the snow field in a cloud model. *J. Climate Appl. Meteor.,* **22,** 1065–1092.

Mapes, B. E., and R. A. Houze, 1995: Diabatic divergence profiles in western Pacific mesoscale convective systems. *J. Atmos. Sci.,* **52,** 1807–1828.

Montgomery, M. T., M. E. Nicholls, T. A. Cram, and A. B. Saunders, 2006: A vortical hot tower route to tropical cyclogenesis. *J. Atmos. Sci.,* **63,** 355–386.

Nguyen, S. V., R. K. Smith, and M. T. Montgomery, 2008: Tropical-cyclone intensification and predictability in three dimensions. *Quart. J. Roy. Meteor. Soc.,* **134,** 563–582.

Otkin, J. A., H.-L. Huang, and A. Seifert, 2006: A comparison of microphysical schemes in the WRF model during a severe

weather event. Preprints, *Seventh Annual WRF Users' Workshop,* Boulder, CO, NCAR, 5 pp. [Available online at http://cimss.ssec.wisc.edu/goes_r/awg/proxy/nwp/gm_publications/Otkin_2006wrf1.pdf.]

Schubert, W. H., and B. T. Alworth, 1987: Evolution of potential vorticity in tropical cyclones. *Quart. J. Roy. Meteor. Soc.,* **113,** 147–162.

Skamarock, W. C., J. B. Klemp, J. Dudhia, D. O. Gill, D. M. Barker, W. Wang, and J. G. Powers, 2005: A description of the Advanced Research WRF version 2. NCAR Tech. Note NCAR/TN-468+STR, 88 pp.

Tao, W. K., J. Simpson, C.-H. Sui, B. Ferrier, S. Lang, J. Scala, M.-D. Chou, and K. Pickering, 1993: Heating, moisture, and water budgets of tropical and midlatitude squall lines: Comparisons and sensitivity to longwave radiation. *J. Atmos. Sci.,* **50,** 673–690.

Wang, Z., M. T. Montgomery, and T. J. Dunkerton, 2009: A dynamically based method for forecasting tropical cyclogenesis location in the Atlantic sector using global model products. *Geophys. Res. Lett.,* **36,** L03801, doi:10.1029/2008GL035586.

——, ——, and ——, 2010: Genesis of pre–Hurricane Felix (2007). Part I: The role of the easterly wave critical layer. *J. Atmos. Sci.,* **67,** 1711–1729.

Wirth, V., and T. J. Dunkerton, 2006: A unified perspective on the dynamics of axisymmetric hurricanes and monsoons. *J. Atmos. Sci.,* **63,** 2529–2547.